Fabrication and characterization of silicon nanowires hybrid Solar cells: A Review

Rabina Bhujel and Bibhu P. Swain

[1]Center for Materials Science and Nanotechnology, Sikkim Manipal Institute of Technology, Majitar, Rangpo, Sikkim, 737136, India.
Corresponding email: bibhuprasad.swain@gmail.com

Abstract. Nowadays hybrid (inorganic-organic) solar cells have become centre for attractive research for their comparatively low cost and fundamental research for prominent organic – inorganic hetero-junction. This review mainly aims to focus on the basic concepts of silicon nanowires (Si-NWs) hybrid solar cells including different fabrication and characterization procedures and the fundamental aspects on which solar cell works. Various techniques have been reported for the synthesis of Si-NWs such as CVD, Oxide assisted growth, Lithography and electro-less metal assisted chemical etching. A further discussion is made on the various characterization procedures such as SEM, TEM, XRD, XPS, UV-Vis, PL, FTIR, Raman and I-V for both Si-NWs and the hybrid solar cell. Furthermore a comparison has also been made between various solar cells with the help of a table showing different Si-NWs hybrid solar cell and their efficiencies.

Keywords: Hybrid solar cell, Si-NWs,Characterization techniques and solar cell efficiency

1. Introduction

The world's energy consumption rate has been elevating continually since the industrialization era. Therefore non-renewable energy resources are becoming limited to fulfil the energy requirement of raising population worldwide. In 2015, the level of world energy consumption was approximately 22 terawatts (TW). Based on the on-going trend of the increase in the energy consumption over the years, it is reported that the world energy consumption will reach up to 28-35 TW by 2050 with an annual increase of 2%. The limited reserves of fossil fuel will not be sufficient enough to supply this high energy demand; therefore there is an immense requirement for clean and renewable energy. Among the various energy resources including bio energy, geothermal energy, wind and hydroelectricity, sunlight is the most abundant and potential natural energy resource. While the estimation shows that the sun has an available renewable energy of 86000 TW per year and sunlight striking the earth in one hour is enough to meet our annual global energy consumption, unfortunately, most of the sunlight energy is lost due to reflection and its absorption by dust and molecules of different gases. Therefore solar cells can be a promising candidate to utilize maximum solar radiations and provide enough energy to fulfil the high-energy demand for the up-coming generation.

In the past few years, hybrid solar cells have attracted tremendous interest of the researchers due to their several advantages like light weight, cost effectiveness, ability to overcome Schokely-Queisser limit, flexibility as well as their capability to produce the photovoltaic device on a large scale. A hybrid solar cell is a mixture of organic and inorganic materials with their combined properties. In Si-NW hybrid solar cells the inorganic material is composed of Si-NWs and organic part constitutes of organic semi-conducting materials such as PEDOT: PSS, P3HT: PCBM, MEH-PPV, spiro-(OMeTED) etc. Recently Si-NWs have become an active component for efficient hybrid solar cells due to their unique structural, electrical and optical properties. In this short review, we will mainly focus on the basic concepts of Si-

NWs hybrid solar cells including their fabrication process, different Si-NWs/ polymer hybrid solar cell structures and various characterization techniques performed for Si-NWs as well as the hybrid solar cells.

1.1 Brief review on 1st, 2nd, 3rd and 4th Gen-eration (G) solar cells
In 1946 Russel Ohl invented a Si wafer based solar cell working on the principle of photovoltaic effect which was discovered by Alexander-Edward Becquerel in 1839. Since then huge efforts have been drawn by the researchers to develop a variety of solar cells for the production of electricity by using solar radiations as a renewable and environment friendly energy resource. On the basis of the materials used, solar cell devices are categorized in many classes as shown in Fig.1.

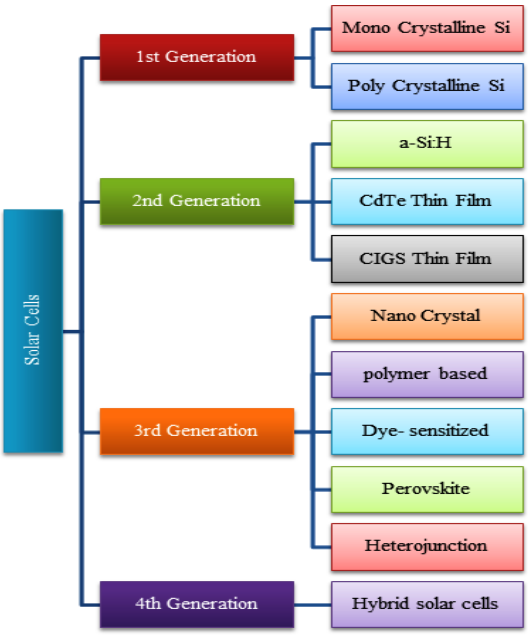

Fig.1 Different generation of solar cells [1-11].

1.1.1 1st Generation (G) Solar cells 1st G Solar cells are also known as wafer based solar cells as they are the basic version of Photovoltaic (PV) devices based on Si wafers. The typically demonstrated efficiency of the 1st G solar cell was around 15-20% but at the same time they were expensive. Commercially these solar cells are in high demand as their efficiency is quite good and has a better lifetime. 1st G solar cell is further divided into two classes:
a) Mono Crystalline Si wafer based Solar Cells[1],
b) Poly Crystalline Si Wafer based Solar Cells [2].

1.1.2 2nd G Solar cells The 2nd G solar cells are based on a thin film of amorphous Si (a-Si), CdTe (cadmium telluride) or CIGS (copper indium gallium diselenide). These solar cells are highly economical as they use a thin layer of photoactive materials of around 1µm thick instead of using a thick wafer. With decreasing the thickness of conducting material the amount of light absorbed gets weaker and hence reduces the efficiency of the solar cell device. The demonstrated efficiency of these solar cells was around 10-15%. 2nd G solar cells have three classes:
a) Amorphous Si Thin Film Solar Cells [3],
b) CdTe Thin film Solar Cells [4] and
c) CIGS Thin Film Solar Cells [5].

1.1.3 3rd G Solar cells 3rd G solar cells include solar cells having high efficiency such as polymer solar cells, multi-junction solar cells and Dye Sensitized solar cells. These solar cells are economical as well as highly efficient. The theoretical efficiency of the 3rd G solar cell is ~80%. These P-V devices also cover multi-junction solar cells which show the capability of overcoming Shockley-Quiesser Limit. These solar cells have been reported to produce the highest practically obtained efficiency of about 46% in the laboratory. 3rd G solar cells have various categories as follows:

a) Nano Crystal solar cells [6],
b) Polymer Based solar cells [7],
c) Dye Sensitized solar cells [8],
d) Perovskite solar cells [9] and
e) Multi junction solar cells [10].

1.1.4 4th G Solar cells 4th G solar cells are the emerging technology in the field of solar cell industry. 4thG solar cells are also known as "organic in inorganic" or Hybrid solar cells [11]. The inorganic material is composed of inorganic nanostructures like Quantum Dots or nanowires and organic material contains conducting polymers such as PEDOT, PPV, Perylene etc. Till date, the highest efficiency achieved by this type of solar cell is around 15%. Because of the various advantages offered by 4th G solar cells they are under extensive research to yield better efficiency in future.

2. Synthesis of Si-NWs

In 1964 Wagner and Ellis first reported the synthesis procedure of Si-NWs via a vapour- liquid- solid (VLS) process by using Au as a catalyst and silane gas as a precursor [12]. Since then various methods have been employed for the synthesis of Si-NWs. Basically, there are two approaches for the fabrication of Si-NWs, i.e. the bottom up and the top down approach. The bottom-up approach is a process of assembling Si nanoparticles to form Si-NWs. This approach includes Oxide assisted growth and vapour-liquid-solid (VLS) growth or solution based growth via CVD. The top-down method includes reduction of bulk Si to Si-NW arrays by Lithography followed by etching and electroless metal-assisted chemical etching (EMACE).

2.1 Bottom up fabrication via chemical vapour deposition

CVD is a commonly used process to synthesize high quality, crystalline, dense and vertically aligned Si-NWs. In this method Au, Ag or Al are used as a catalyst and Silane or Si tetrachloride serves as a precursor gas. As a result of the different chemical reactions taking place on the surface of the substrate, it gets covered with a fine layer of Si-NWs. CVD offers an epitaxial growth of Si-NWs depending upon the precursor used and the reaction conditions. By changing the growth velocity from 10^{-2}-10^{3} nm min^{-1} Si-NWs with varying length and diameter can be achieved. The CVD process is further dived into many classes based upon the reaction parameters and the Si precursor used.

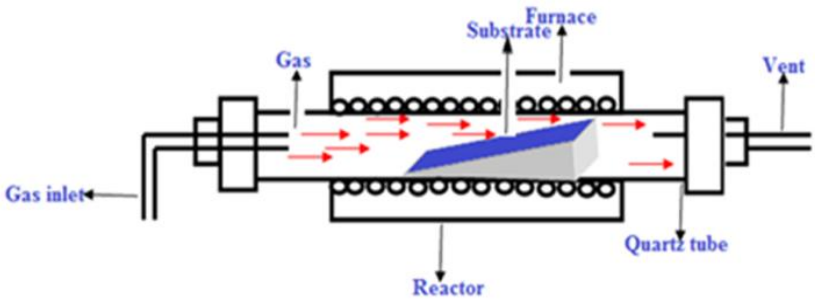

Fig. 2 Schematic of APCVD reactor used for Si-NWs fabrication.

An atmospheric pressure chemical vapour deposition (APCVD) process has been used to prepare hetero-structural NiS/SiO_2 nanowire/nanotubes (NW/NTs) with an average diameter of 50 nm and length of 10 mm on a Si substrate as reported by Ge et al [13].Swain et al. fabricated vertically aligned Si-NWs by annealing the Au sputtered Si substrate at a temperature of about 700°C for around 100-120 minutes in an APCVD reactor [14]. The Si-NWs with diameters below 3 nm can also be achieved by using a low-pressure chemical vapour deposition (LPCVD) reactor. In this technique most commonly SiH_4 is used as a precursor and H_2 as a carrier gas [15], [16] for the fabrication of Si-NWs. The surface of the NW is passivated to reduce the surface roughness and to obtain better results. VLS-CVD technique is one of the most commonly used technique to produce vertically aligned Si-NWs [17], [18] using SiH_4 or $SiCl_4$ as a precursor gas. The HCl produced during the decomposition of $SiCl_4$ is responsible to etch the Si surface for producing desired Si-NWs. Si-NWs can also be synthesized using a PECVD reactor [19]. Yu et al. reporteda Bi catalysed growth of Si-NWs by following VLS growth technique in a PECVD reactor[20]. The SEM image in Fig.3 c) shows that the density of Si-NWs Solely depends upon the catalyst used. With decreasing the initial Bi thickness, the produced Si-NWs become smaller with increasing density.

2.1.1 Oxide Assisted Growth (OAG) It is a method used to grow pure Si-NWs using oxides instead of metals as a catalyst. Oxides play an important role in inducing the growth of Si-NWs. OAG process allows large area fabrication of Si-NWs with controlled size and diameter.Hutagalung et al. successfully synthesized Si-NWs with the diameter ranging from 10–90 nm by OAG mechanism with carbo-thermal evaporation method [21]. By setting the furnace system at 20ºC per min to 110ºC for 6 h, the vertically aligned crooked Si-NWs were achieved on the silicon substrate placed 12 cm away from the source material.Sphere capped Si-NWs were also obtained indicating the presence of silicon oxide. Davenas et al. synthesized Si-NWs by using OAG mechanism based on a dismutation reaction of the silicon monoxide formed from the mixture of Si and SiO_2 at 1200°C without using any catalyst[22]. The diameter of Si-NWs was less than 20 nm and length was about 10μm.

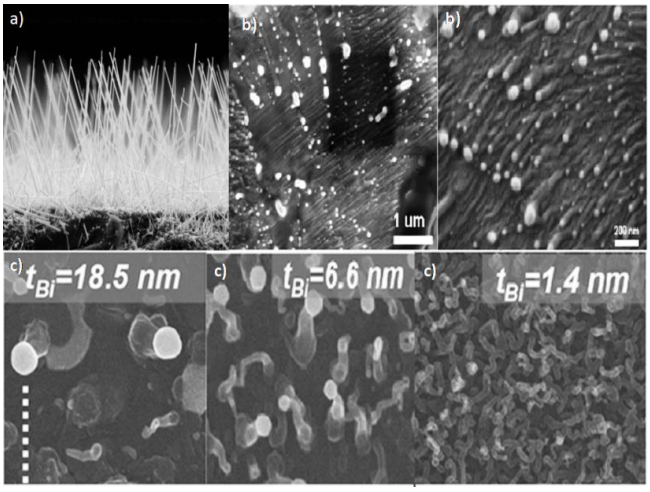

Fig.3 a) Cross-sectional SEM images of Si-NWs synthesized by CVD [18]. 3 b) Fig.6 b) SEM images of vertical aligned Si-NWs and crooked grown Si-NWs [21]. Fig.5Top-view SEM images of Si-NWs[19].

2.2 Top- Down fabrication

The top down fabrication of Si-NWs include Lithography and EMACE method.

2.2.1 Lithography followed by etching Lithography is one of the most common and the oldest way of depositing metal nanoparticles for the synthesis of Si-NWs followed by etching. It is widely used for producing vertically aligned Si-NWs on a large scale. Wang et al. fabricated Si nanopillar arrays (NPAs) via catalytic wet etching combined with colloidal lithography[23]. At first Ag colloidal particles were deposited on the surface of Si substrate which serves as a catalyst. The NPA structures were achieved by the subsequent catalytic wet etching with Ag patterns. The NPA with a diameter ranging 180-325 nm and length of 2.2μm were obtained. Peng et al. Also used lithography technique for the deposition of Si colloidal particles for the synthesis of Si-NWs by electro-less etching[24]. Si-NWs with good characteristics were obtained as shown by the SEM images in Fig.4

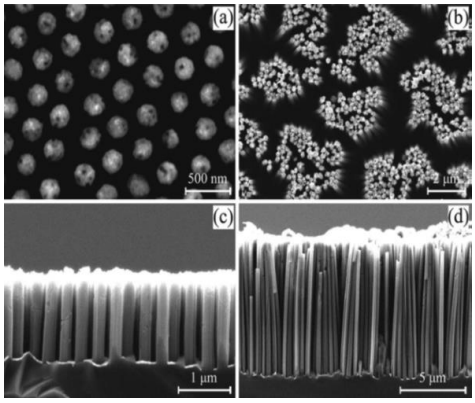

Fig.4 a) and b) shows top-view SEM images of vertically alignedorderedSi-NWs produced on p-type Si(100) and p-type (111) substrates etched in HF–H_2O_2 for 5 and 15 min, respectively.c) and d) are Cross sectional views of Si-NWs in a and b, respectively [24].

2.2.2 Electroless metal-assisted chemical etching (EMACE)
Among the various techniques applied for the synthesis of Si-NWs, EMACE is the simplest, low temperature and a cost effective way to obtain vertically well-aligned Si-NWswith a high aspect ratio over large areas. Various metals such as Au, Ag, Sn and Al can be used as a catalyst.

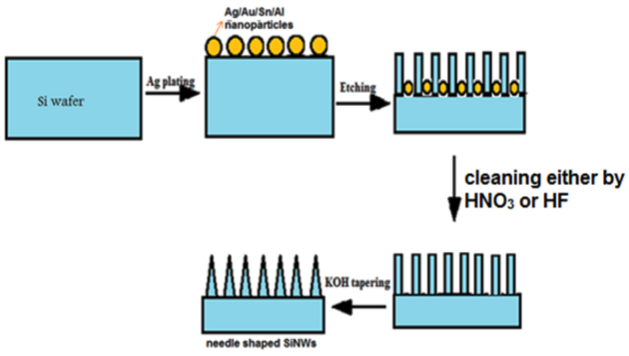

Fig.5 Schematic figure of the steps followed in EMACE method.

In 2002, Penget al. reported the synthesis of large-scale Si-NW arrays by simply dipping the Si wafer in a solution of HF and $AgNO_3$ at room temperature[25]. Since then various attempts has been done to

produce Si-NWs with varying diameter and length for obtaining better performance regarding absorption of solar radiation. Bai et al. followed electro-less etching method for the synthesis of Si-NWs by using Ag as a catalyst [26]. Ag nanoparticles were deposited on Si surface by sputtering techniques. The Si-NW arrays of 400 nm thickness showed the lowest average reflectance of 1.6% for wavelengths ranging from 300 to 1000 nm. Gong et al. synthesized needle shaped Si-NWs by tapering the etched Si substrate in a 30% NaOH solution [27]. The NaOH tapered Si-NWs showed higher absorption as compared to the untapered one. Kurokawa et al. followed a DR process for the band gap tuning of Si-NWs with a diameter of 30 nm and a length of 15μm, in which H_3PO_4 oxidation and HF etching were repeated several times[28]. Jiang et al. synthesized Si-NWs by the EMACE method with potassium permanganate ($KMnO_4$) as an oxidizing agent [29]. The hybrid solar cell fabricated by these Si-NWs presented an increase of 0.72mA/ cm^2 in the short-circuit current density comparing with H_2O_2 as an anisotropic oxidizing agent. Jung et al. suggested cost effective way to fabricate the Si-NWs for commercial solar cell application[30]. Vertically aligned Si-NWs were prepared by metal-assisted chemical etching, followed by KOH tapering to enhance the optical absorption. The tapered NW solar cell showed ~23% increase in a short circuit current and 80% increase in conversion efficiency compared to bunch nanowires. Jeon et al. synthesized Tin-catalysed Si-NWs by electroless etching method for solar cells application [31]. The reflectance of as synthesized silicon nanowires was obtained approximately 5% in the short wavelength region (λ_b500 nm). Similarly Hakan karaagac[32], Kim et al.[33], Jiang et al. [34] and Kalita et al.[35] also followed the same procedure by using Ag as a catalyst for the synthesis of Si-NWs for solar cell application.

3. Characterization of Si-NWs

The papers over past decade show that several characterization techniques have been employed for Si-NWs. The morphology of Si-NWs was characterized by SEM and TEM, structural characterization was done by XRD. The vibration and bonding network of the Si-NWs were shown by FTIR and Raman spectroscopy and the core orbital information and the functional group of Si-NWs were characterized by XPS.

3.1. Morphology of Si-NWs

In order to evaluate the performance of a solar cell device, it is important to obtain the length and diameter of Si-NWs in a growth matrix. Such a morphological study of Si-NWs is generally carried out with the help of Scanning electron microscopy (SEM) [32, 36] and transmission electron microscopy (TEM).

*3.1.1 Scanning electron microscopy (SEM***)** SEM is a type of electronic microscope that images the surface of a sample with a focused high energy beam of electrons in a raster scan pattern. The electrons interacts with the atoms present on the surface of the sample and produces various signals such as secondary electrons, back scattered electrons (BSE), characteristic X-rays, visible light and heat. Secondary electrons are important to show the morphology of the sample whereas backscattered electrons are responsible for producing information about the composition of the sample. The topographic image obtained by the detection of secondary electrons helps in evaluating the length and diameter of synthesized Si-NWs.Peng et al. performed FE-SEM characterization to show the morphology of Si-NWs synthesized by Electro-less etching method [37]. The SEM images showed that the diameter of Si-NWs was in the range of 20-300 nm, and the axial wire length was about 17μm. Syu et al. showed the top and 45° tilted side SEM images of Si-NW arrays with the wire lengths of about 0.42, 2.15 and 5.59μm [38]. The cross sectional FE-SEM images obtained by Pham et al. Showed vertically aligned Si-NW arrays with different lengths of 4μm, 6μm and 8μmfor different reaction times of 30min, 45min and 6 min respectively at room temperature [39].

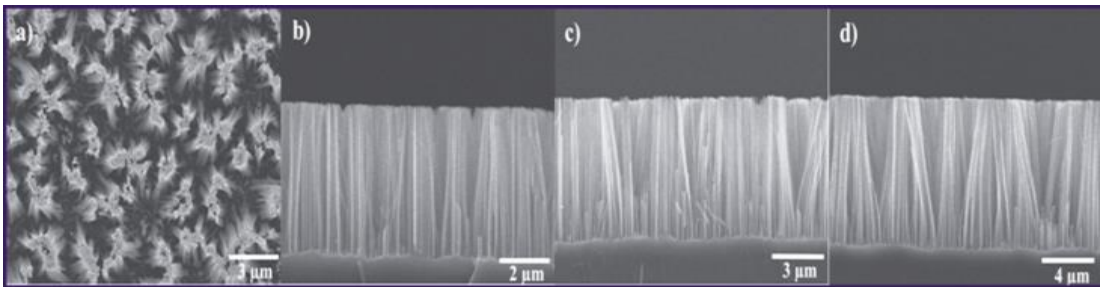

Fig.6(a) Top-view SEM image of p-type Si-NWs; cross-sectional SEM images of Si-NWs with different length (b) 4µm, (c) 6µm and (d) 8µm corresponding to 30 min, 45 min and 60 min etching times, respectively[39].

3.1.2 Transmission Electron Microscopy (TEM) TEM is an extremely useful electron microscopy technique used to obtain the image of an ultrathin sample with the help of a beam of electrons transmitted through it. The images are obtained due to the interaction of transmitted electrons with the atoms present on the sample. TEM can be used to analyse the composition and the defects present in the sample. The shape, size, quality and density of nanowires or quantum dots can also be evaluated with the help of high resolution TEM. Kalita et al. observed that the diameter of Si-NWs synthesized by electroless etching method varied from 20-150 nm [35]. From the cross-sectional TEM image Kurokawa et al. showed that the diameter of Si-NW arrays around the tip was reduced by around 5 nm [28].

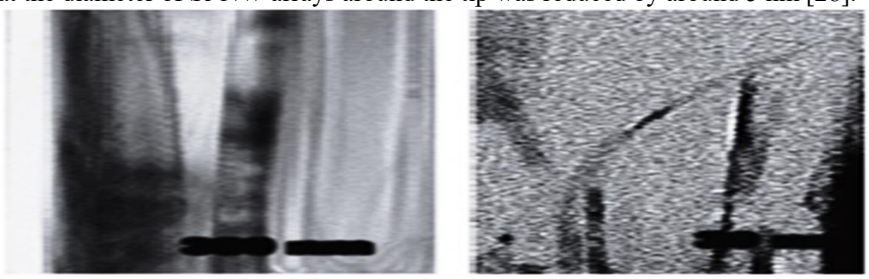
Fig.7 TEM image of SiNWs

3.2 Structural characterization of Si-NWs using X-ray diffraction Technique
The structural characterization of Si-NWs has been done by X-ray diffraction (XRD) technique, which gives an idea about the crystallite size, structure and its chemical composition. This technique is based on the constructive interference between the monochromatic X-rays and a crystalline sample. The interaction of the incident rays with the sample generates fingerprint patterns as a result of the constructive interference as explained by Bragg's equation.
$n\lambda = 2dsin$.....(1)
This equation determines the angle θ, under which the first, second, third……order reflection occurs, for n=1,2,3…..
The XRD pattern obtained by Miao et al. for Pt/Si-NWs shows peak position for Pt at (111), (200), (220) planes and peak for Si is at (004) plane which is shown in fig.8 (a)[40]. From the XRD characterization of Ag deposited Si-NWs shown in fig.8 (b), Liu et al. found that the peaks for Ag-NPs were coming at (111), (200), (220), (311) and (222) planes[11]. The peak for Si-NWs was at (400) plane. Kim et al. observed the (111), (200), and (220) crystal planes at 2θ degrees of 37.31°, 43.31° and 62.91°, respectively[33].

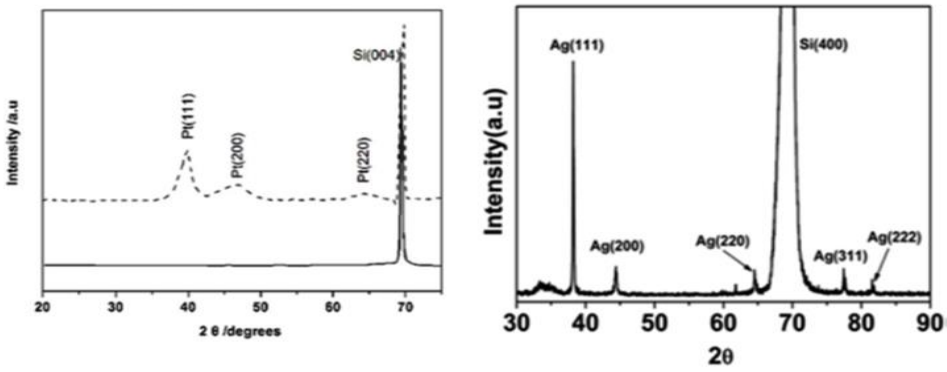

Fig. 8 XRD spectrum of Pt/Si-NWs[40] and Ag-NPs on Si-NW array [11].

3.3 Compositional characterization of Si-NWs

Compositional characterization of Si-NWs has been done by XPS(X-Ray photo electron spectroscopy) technique to show the functional groups and chemical oxidation states present in Si-NWs.It is based on the photo electric effect as explained by Albert Einstein. The atoms present on the surface of the samples are excited with the X-Rays causing the photo electrons to be emitted from the sample surface. The energy of the emitted electron is measured with the help of a photo electron spectra obtained by an electron energy analyser. The analysis of binding energy and intensity of the peak detects the constituents present in the sample. Kim et al. investigated the functional groups and chemical oxidation states present in the nickel oxide Si-NW/C as shown in Fig.9[33]. The XPS spectra in Fig.9 a shows a comparison of the Si-NW/C with and without NiO decoration. Peaks corresponding to Si-2p, C-1s, and O-1s were obtained for both the Si-NW/C and NiOSi-NW/C, and a peak corresponding to Ni-2p was only present in the NiOSi-NW/C, which indicates that the NiO was decorated on the surface of the carbon shell.From the XPS analysis of Si-NWs synthesized using Sn as a catalyst, Jeon et al. detected that both Sn metal and Sn oxide were at 484.9 and 487.2 eV of binding energy respectively[41]. Also Sn oxide has higher counts than Sn. As HCl dipping time increases, Sn and Sn oxide counts were decreased.

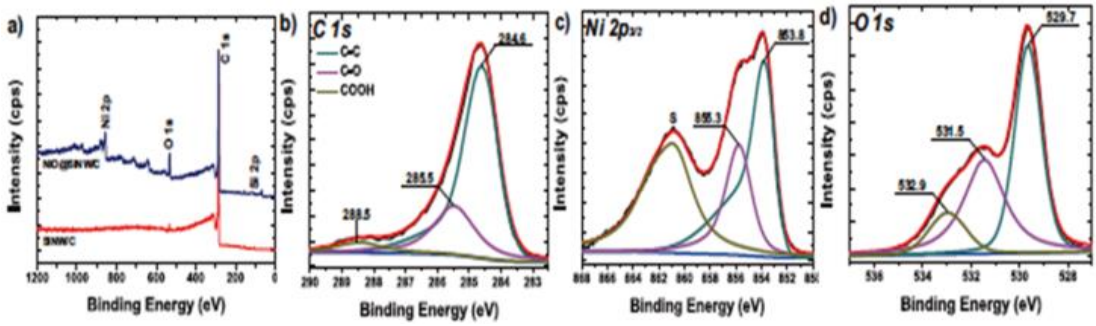

Fig.9 X-ray photoelectron spectroscopy spectra for Si-NW/C and NiOSi-NW/C: a) survey scan, b) high-resolution C 1s spectrum, c) high-resolution Ni 2p3⁄2 spectrum, and d) high-resolution O 1s spectrum for NiOSi-NW/C [33].

3.4 Optical properties of Si-NWs

The optical properties of Si-NWs are characterizedeitherby UV-Vis or photoluminescence spectroscopy.

3.4.1 UV-Vis characterization of Si-NWs UV-Visible (UV-Vis) spectroscopy refers to the absorption or reflectance spectroscopy in the ultraviolet and visible region due to the excitation of electrons from

valence band to conduction band or from highest occupied molecular orbital (HOMO) to lowest unocupied molecular orbital (LUMO) respectively.Syu et al. studied the reflectivity of Si-NW arrays length of 0.42μm, 2.15μm and 5.59μm and planar Si wafers and concluded that Si-NWs arrays make the reflectance under 5% in the visible range, while single polished planar Si wafers has the reflectance more than 35% in the range of visible light and infrared [37]. On the other hand, reflectance increase while nanowire length decrease. It indicates that light trapping ability is better for longer Si-NWs which is shown by the Fig.10

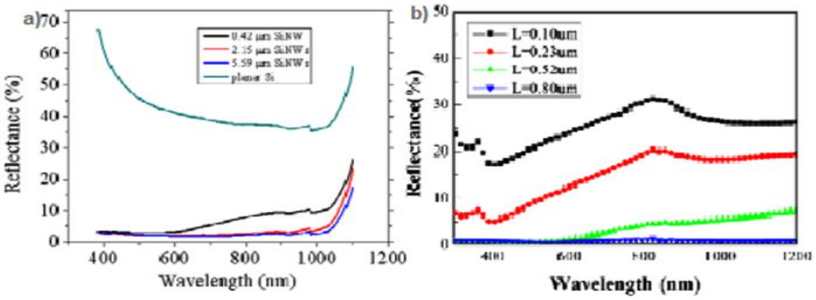

Fig.10 (a) Reflectance of 0.42μm, 2.15μm and 5.59μmSi-NW arrays and planar Si in the spectral range from 380nm to 1100nm[37], (b)The reflectance spectra of Si-NW arrays [13].

Woo et al. observed similar observation for reflectance of Si-NW arrays about 2–5% as compared with the bare ITO glass[42]. This means that the devices containing Si-NWs have the potential to exhibit enhanced absorption due to the suppression of reflection and enhancement of light trapping in the visible range. Ashour et al. found that the length of Si-NWs increases linearly with etching time[43]. By UV-Visible spectra they concluded that the best reflectance is obtained when the etching time is 80 min with an effective reflectivity of 2.5 % (between 250 and1000nm).In order to obtain Si-NWs with different diameters Yu et al. modified Si-NWs dimensions by changing thermal oxidation and HF acid etching time[44]. The reflectivity of Si-NWs monotonically decreases with thermal oxidization time and reached minimum value of ~3% at 180 min. however, the reflectance increases to ~6% with of thermal oxidization time of 600 min in the entire light wavelength.Ge et al. investigated the effect of wire length in the Si-NWs and observed that the reflectance decreases with increasing the wire's length as shown in fig.10 b)[13].

3.4.2 Photoluminescence (PL) characterization of Si-NWs The PL characterization is an important tool to obtain the optical properties of surface states and bulk states, and electronic structure such as density of states of the Si-NWs. In the PL characterization technique the photo excitation causes the electron to jump from lower energy level to the higher excited levels. When these excited electrons return back to its stable state it releases energy in terms of light. Davenas et al. found that the absorption edge of the Si-NWs (at 364 nm) shows a strong PL band at 860 nm (Fig.11) at room temperature showing an electronic confinement effect due to the increase in the band gap energy of the material[22].

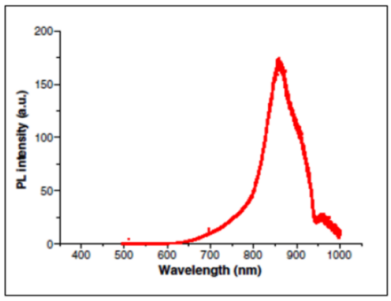

Fig.11Photoluminescence band at 860 nm of HF etched Si-NWs [22].

3.5 Vibration and bonding of Si-NWs

The vibration and bonding present in Si-NWs are characterized by Raman and FTIR spectroscopy, which shows the presence of impurity in the Si-NWs.

3.5.1 Raman spectroscopy Raman spectroscopy is based on the inelastic scattering of monochromatic light near visible or ultra-violet region. Davenas et al. deduced the doping type of the nanosilicon phase in Si-NWs from the a Raman peak which results from the perturbation of the phonon scattering due to the excitation of the electrons in the conduction band[22]. N-type doping was concluded from the Fanoresonance appearing on Fig. 12 on the low wavenumber side of the Raman peak at 500 cm^{-1}. Kim et al. examined the intensity ratios of different peaks to investigate the quality of the carbon shell and the degree of defects present in Si-NWs with the help of Raman analysis[33].

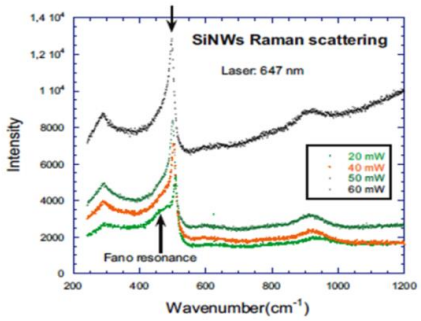

Fig.12 Fano resonance of SiNWs Raman spectrum with various beam power [22].

3.5.2 FTIR spectroscopy of Si-NWs FTIR analysis shows the presence of impurity states, diffrent chemical bonding and functional groups of Si-NWs. Lin et al. observed that the asymmetric stretching signal of Si–O–Si bridge is distributed between 1,000 and 1,300 cm^{-1} in the Si-NWs[45]. The peaks between 2,050 and 2170 cm^{-1} represent the absorption due to Si–H and Si-H_2 stretching, while the peak at 2,248 cm^{-1} corresponds to the Si–H_3 stretching mode in O_3-SiH. The signal for Si–O bond is much stronger for the HNO_3 treated sample as compared to the HF treated one. The small peaks around 2,100 and 2,248 cm^{-1} indicated the presence of small amount of surface hydrogen bonds. Amri et al. [46] analysed the FTIR absorption spectra of Si-NWs to study the effect of molar ratio (H_2O_2) variation on the surface composition of porous micro-cavities. The bending and asymmetric stretching mode of Si-O-Sibands is localized at 460 and 1080 cm^{-1}, respectively. Furthermore, the appearance of O_3Si-H and Si-O-H modes situated at 2276 and 3640 cm^{-1} might be explained by the incorporation of oxygen in the Si-Si-H bands and its evolution to O_x-Si-H_y bands.

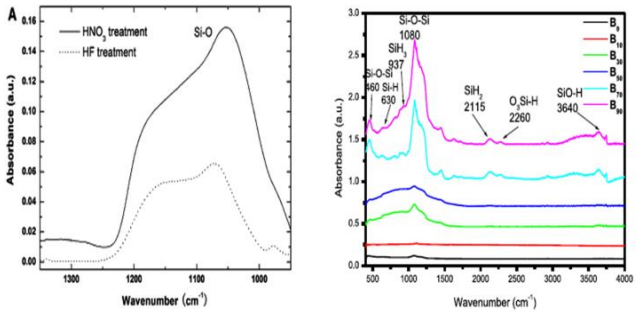

Fig.13 FTIR spectra of the Si-NWs treated with HNO_3 and HF [45] and FTIR spectra obtained by Amri et al [46].

4. Si-NWs Hybrid Solar Cell Device Structure

Generally hybrid solar cells are planar in nature consisting of a photo active layer of semiconducting material sandwiched in between the electrodes of different work function. A layer of conducting polymer such as PEDOT:PSS, P_3HT:PCBM etc is coated on the surface of the photoactive layer to form a hetero-junction. The device is built on a transparent substrate such as glass and the anode consists of ITO, a semi-transparent conducting material to allow maximum light to pass through the solar cell as to increase the efficiency. ITO is also responsible for collecting holes generated on the solar cell device. Also metals such as Ag, Al or Ti, can be used as the anode instead of using ITO. In past few years various attempts has been done by the researchers to improve the efficiency of hybrid solar cells. Among the different inorganic materials used,Si-NWs obtained the best result combined with PEDOT:PSS as the organic semiconducting material. The band gap energy of Si-NWs and different polymers are responsible for producing photo current by restricting the recombination of the charge carriers.Yu et al. Produced a theoretical efficiency of around 31.11% as demonstrated by a PEDOT:PSS/ Si-NWshybrid solar cell whereas Syu et al. showed an actual efficiency of around 13% in laboratory also for the PEDOT:PSS/Si-NW hybrid solar cell.

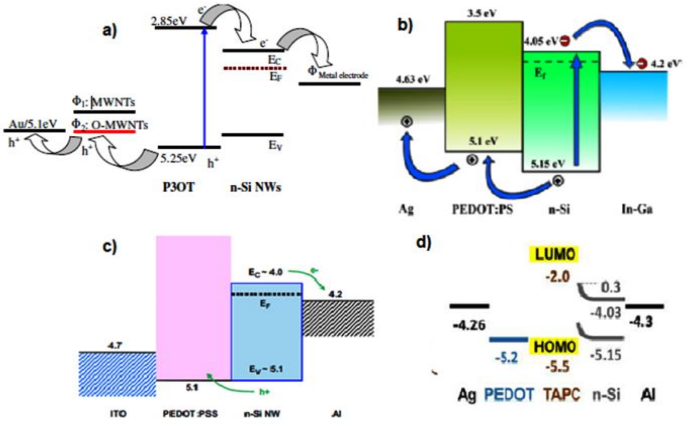

Fig.14 Energy band diagram of different Si-NWs hybrid solar cell as shown by a) [35]. b) [65] c)[42] and d) [56].

4.1 Si-NWs/PEDOT: PSS hybrid solar cell

Bai et al. fabricated a heterojunction Si-NW hybrid solar cell using PEDOT:PSS as a conducting polymer and obtained a short circuit current (Isc) of 25.15 mA cm^{-1} and power conversion efficiency (PCE) of 6.72% [26]. Sato et al. designed a high performance and low-cost radial hetero-junction solar cell by combining vertically alligned n-type Si-NWs with PEDOT:PSS as polymeric layer [47]. The solar cell consisting of NW arrays with the length of 0.57mm and Ag finger grid electrode with the thickness of 100nm achieved a PCE of 9.3% showing the best cell performance. Sharma et al. fabricated an organic-inorganic hybrid solar cell containing KOH tapered Si-NW arrays with Ag-NPs (silver nanoparticles) and PEDOT:PSS polymeric layer [48]. The Ag-NPs showed a plasmonic back scattering effect which contibuted towards the 10% enhancement in the PCE of the solar cell device. Wang et al. provided a comparative study between a solar cell device with and without evacuating the PEDOT:PSS layer on top of the Si-NW arrays [49]. The evacuated solar cell obtained better PCE of 9.22% as compared to the untreated pristine one having a PCE of 5.17%. Syu et al. fabricated a Si-NW/hybrid solar cell with zonyl fluoro surfactant treated PEDOT:PSS and obtained a PCE of around 9.18% [50]. The zonyl fluoro surfactant treatment on PEDOT:PSS helped improving the affinity between PEDOT:PSS and Si-NW arrays in the solar cell device which was further responsible for improving the cell performance . Uma et al. studied the effect of graphene oxide (GO) on the performance of a Si-NWs/PEDOT:PSS blended hybrid solar cell [51]. The GO blended solar cell showed enhanced light trapping with the PCE of about 9.57% under the AM 1.5G condition. Yu et al. obtained a PCE of around 13% for an organic/Si-NWs hybrid solar cells with (PEDOT:PSS) and low filling ratio Si-NWs (LF-Si-NWs) having low reflectance property[44].

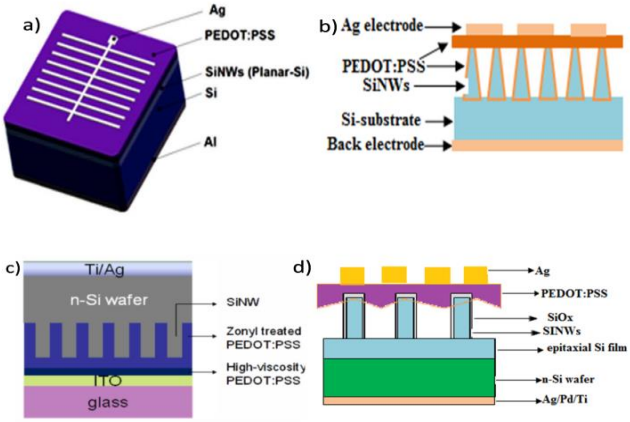

Fig.15 Various Si-NWs/PEDOT:PSS hybrid solar cells a) [44], b) [26], c) [50] and d) [55].

Wang et al. demonstrated a two-step surface treatment process to obtain high efficiency Si-NW/PEDOT:PSS hybrid cells[52]. The Si-NWs were first treated with ozone plasma to form a surface sacrificial oxide, followed by an HF etching process to partially remove the oxide. The surface treated Si/PEDOT:PSS hybrid solar cell showed the V_{oc} of 0.58 V and a PCE of 12.4%. Gong et al. Showed a comparative study between hybrid solar cell device based on the NaOH tapered and untapered Si-NW array [53]. The PCE of 6.87% was achieved for the tapered Si-NWs/PEDOT:PSS hybrid cell with an optimized Si-NWs length of 0.45µm. Shen et al. demonstrated a Au-NPs incorporated SiNW/PEDOT:PSS hybrid solar cell and obtained a PCE of about 12.85%, which was 23% higher than that of the pristine one containing no Ag-NPs [54]. Wang et al. fabricated (Ag/PEDOT:PSS/SiOx-Si-NWs/ Epitaxial Si/n-Si/Ag or Pd or Ti) hybrid solar cell on a 10.6µm-thick crystalline Si thin films with the surface treatment process using oxygen plasma to improve the surface quality of the Si-NWs[55]. The surface treatment process was performed to remove surface defects and substantially improve the average open circuit voltage from 0.461 to 0.562 V. The optimized solar cell with 0.7-µm-long Si-NWs

achieved a power conversion efficiency (PCE) of 7.83 %.Yu et al. demonstrated a hybrid hetero-junction solar cell based on Si-NWs, PEDOT:PSS and an intermediate thin layer of 1,1-bis [(di-4-tolyl amino) phenyl] cyclohexane (TAPC) and obtained a power conversion efficiency of 13.01%[56]. The TAPC layer was attributed to improve the morphology of PEDOT:PSS layer on the top of Si-NWs. Wei et al. Fabricated an Ag/ PEDOT:PSS/Si-NWs/Al hybrid solar cell consisting of micro pyramid hierarchical structures showing an outstanding solar cell efficiency of around 11.48% [57]. Syu et al. demonstrated that the Si-NW/PEDOT:PSS solar cell with the shortest wavelength of 0.37mmobtained a PCE of 8.40%, as compared to the solar cell having different wire lengths [58].

4.2 Si-NW:PCBM hybrid solar cell

Hakan karaagac fabricated an Al/p-Si-NW/PCBM/ITO hybrid solar cell based on Si-NWs as the inorganic material and PCBM as the organic conducting polymer [32]. The current–voltage and capacitance–voltage measurements showed that the hybrid solar cell obtained a V_{oc} of 0.19V , J_{sc} of 8.1mA/cm^2, FF around 27 % and finally the PCE of 0.41%.

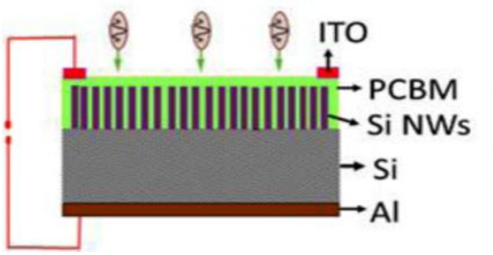

Fig.16 Schematic representation of the fabricated hybrid solar cell [32].

4.3 Si-NWs polymer hetero-junctionsolar cells

Jeon et al. demonstrated the efficiency improvement of hybrid solar cells based on acid treated Si-NWs and organic materials[41]. The removal of Sn and Sn oxide resulted in the increase of open-circuit voltage and shunt resistance which further contributed towards the enhancement of the hybrid solar cell performance. HCl improved shunt resistance and reduced strap-assisted recombination by residual catalyst removal whereas native oxide removal was done by hydrofluoric acid. Both acid treatments lead in increase of power conversion efficiency from 0.35 to 1.5% providing the importance of surface treatment of Si-NWs to obtain efficient hybrid solar cells. Devenas et al. fabricated ITO/PEDOT-PSS/P3HT:Si-NWs/Al hybrid solar cell based on Si-NWs dispersion on PEDOT:PSS thin films as semiconducting material [22]. The Si-NWs were produced by the vapour–solid technique without the use of any metal catalyst. An open circuit voltage of 0.68 V was deduced from the electrical characteristics under visible light illumination.Dkhil et al. fabricated ITO/PEDOT:PSS/Si-NWs:PVK/Al and ITO/PEDOT:PSS/Si-NWs:MEH-PPV/Al solar cell structures and studied the photovoltaic effect by current–voltage (I–V) measurements in dark and under illumination and interpretedon the basis of the charge transfer differences resulting from the morphologies [59].The best parameters like short-circuit current density (Jsc = 0.236×10^6 A cm^2),fill factor (FF = 0.36) and open-circuit voltage (Voc = 0. 48V) were found for the Si-NWs:PVK nano-composite. He et al. reported a cost effective and highly efficient hybrid solar cell based on well-aligned crystalline silicon nanorods (Si-NRs) and an organic semiconductor, 2,2,7,7-Tetrakis (N,N-di-4-methoxy phenyl amino)-9,9-spiro bifluorene (Spiro-OMeTAD), in a core-sheath hetero-junction structure. The device was formed by spin coating Spiro-OMeTAD on Si-NRs array fabricated by electro-less chemical etching. A power conversion efficiency of 10.3% was obtained for a 1-cm^2 cell with 0.35μm long Si-NRs. Shen et al. demonstrated the organic-inorganic solar cell based on hybrid composites of conjugated molecules and Si-NWs on a planar substrate [61]. The In:Ga/Si-NWs/spiro-OMeTAD/Cu/PEDOT:PSS /Cu:Ag solar cell yielded an excellent PCE of around 9.70%. Eisenhawer et al. fabricated a Si-NWs/P_3HT: PCBM

solar cell with the cell efficiency of about 4.2% [62]. The solar cell showed a relative improvement of 10% as compared to a reference cell produced without nanowires due to the enhancement of the electron transport properties imposed by the Si-NWs. Chehata et al. used MEH-PPV polymer matrix with Si-NWs for the hybrid solar cell fabrication and produced a PCE of 5.1%[63]. Different amounts of Si-NWs have been introduced into MEH-PPV polymer matrix and found that the optimum composition of MEH-PPV:Si-NWs (1:2) contribute towards the iomproved absorption and the transport charge processes within the device. Huang et al. fabricated a hybrid solar cell on the glass substrate using well-aligned single-crystalline Si-NWs and P_3HT:PCBM[64]. The organic photovoltaic hybrid cell showed improved performance by increasing the short-circuit current densityfrom 7.17 to 11.61mA/cm^2 and PCE from 1.21% to 1.91%. Kalita et al. presented a simple and novel approach of fabricating three dimensional (3D) n-type Si-NWs and poly(3-octylthiophene) hybrid solar cells incorporating carbon nanotubes (CNTs) and obtained V_{oc}, J_{sc}, FF and PCE as 0.353, 7.85mA/cm^2, 22% and 0.61%, respectively [35].

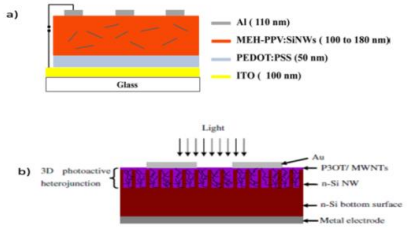

Fig.17 device structure of Si-NWs/polymer hetero-junction solar cell a) [63]and b) [35].

5. I-V characterization for Si-NWs hybrid solar cell

I-V characterization is an important technique to find out the efficiency of a solar cell device in terms of the obtained I-V curve. The values of V_{oc}, I_{sc}, V_m and $I_m$obtained by I-V curve gives the PCE of a solar cell as calculated by the equation 5 and 6.Chehata et al. obtained a J_{sc} of 0.328 A/cm^2, a V_{oc} of 0.680 V and FF of 38% for ITO/PEDOT:PSS/MEH-PPV:Si-NWs (1:2)/Al solar cell as shown by the I-V curve[63].For an Al/n-Si/Si-NWs/Ag-NPs/P3HT:PCBM/PEDOT:PSS/ITO/Glass hybrid solar cell Liu et al. obtained best results with a J_{sc} of 16.6, V_{oc} of .455, FF of 3.23% and PCE of 3.23% for a 26 nm Ag-NPs decorated Si-NWs as shown by the I-V curve[11]. From the fabricated Al/p-Si NW/PCBM/ITO structured hybrid solar cell Kraagacobtained the V_{oc}, I_{sc}, FF, and PCE as 0.19 V, 8.1mAcm^2, 27 and 0.41%, respectively[32].

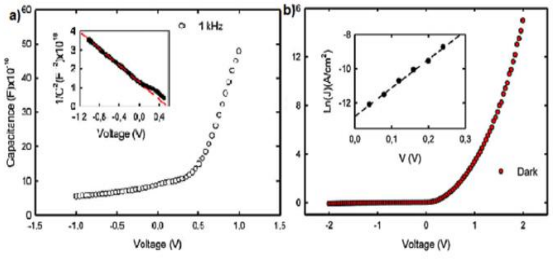

Fig.18 a)C–V characteristic of the device measured at 1 kHz. b) I–V characteristic of the p-SiNW/PCBM in dark condition [32].

Jeon et al. showed the performance of HCl treated Glass/ITO/P_3HT:PCBM/Si-NWs/back electrode solar cell from the I-V characteristic curve[31]. The best result was obtained by 20 min HCl treated solar cell under 13mW/cm^2 intensities of AM 1.5 illuminations. Yu et al. showed that the best results were obtained for TAPC containing Ag/PEDOT:PSS/Si-NWs/n-Si/Al solar cell with anI_{sc} of 34.81mA/cm^2, V_{oc} of 0.54 V and PCE of 13% as shown by the I-V characteristic curve[56].From the I-V curve obtained Shen et al. showed that 15% Au-NPs decorated Si-NWs produced better results. The V_{oc}, I_{sc} and PCE of the fabricated solar cell were 0.622V, 27.70 mA/cm^2 and 12.85% respectively[61].

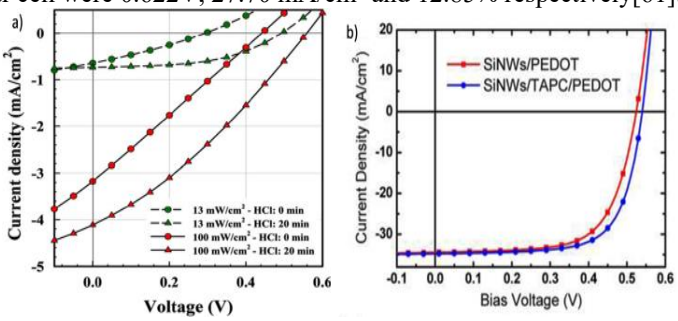

Fig.19 Current density-voltage characteristics of different hybrid solar cells [31, 56].

Table 1 Different Hybrid solar cells with their efficiencies:-

SL	DEVICE STRUCTURE [ref.]	Voc(V), Isc(mA cm^{-1})	FF(%), η(%)
1	Ag/Si-N/PEDOT:PSS/Ag[26]	0.466, 25.15	57.45, 6.72
2	Au/P_3OT/MWNTs/N-Si-NWs/n-Si/metal electrode [35]	0.35, 7.85	22, 0.61
3	Al/Si-NWs/P_3HT:PCB /PEDOT:PSS/ITO [64]	0.45, 11.61	39, 1.91
4	ITO/EPEDOT:PSS/Si-NWsGPEDOT:PSS/aSi:H/ZnO/Al [11]	0.47, 22.89	43.5, 4.68
5	Al/p Si- NW/PCBM/ITO [32]	0.19, 8.1	27, 0.41
6	Glass/ITO/P_3HT:PCBM/Si-NWs/back electrode[41]	0.49, 0.74	50.8, 1.41
7	Ag/PEDOT:PSS/TAPC/Si-NWs/n-Si/Al[56]	0.54, 34.81	68, 13
8	ITO/PEDOT:PSS/MEH-PPV:Si-NWs(1:2)/Al[63]	0.68, 0.328	38, 5.6
9	Ti,Ag/n-Si/Si-NWs:0.1% Zonyl treated PEDOT:PSS/ higher viscous PEDOT: PSS /ITO/Glass [50]	0.531, 26.23	65.92, 9.18
10	Ag/PEDOT:PSS/n-Si/Ag:ALD/Ni,Ag[48]	0.545, 18.50	65.5, 6.62
11	Ti,Ag/Si-NW/PEDOT:PSS-GO(30%)/ITO/Glass[51]	0.518, 31.0	59.6, 9.57
12	Ag/PEDOT:PSS/LF-Si-NWs/Si/Al [44]	0.614, 30.42	70, 31.11
13	Ag/PEDOT:PSS:Si-NWs/n-Si/Al [52]	0.48, 32.99	58.2, 9.22
14	Ag/10% DMSO treated PEDOT:PSS/μ text Si/n-Si/ In-Ga [65]	0.424, 27.2	55.82, 6.45
15	Ag/PEDOT:PSS/15%Au-NPS:Si-NWs/Al [61]	0.622, 27.70	74.6, 12.85
16	Ag/PEDOT:PSS/Si-NWs/Tior Ag [66]	25, 0.55	60.4, 8.3

6. Conclusion

Si-NWs play a crucial role in the field of hybrid solar cell technology because of its superior properties for showing better efficiency to the solar cell devices. The most common and the easiest way of synthesizing Si-NWs is the electroless metal assisted chemical etching method, where Si-NWs are obtained as a result of some redox chemical reactions undergoing in a Teflon vessel.Si-NWs have been characterized by various techniques such as SEM, TEM, XRD, XPS, RAMAN, UV-VIS and FTIR to know its various properties.Considering Si-NWs as an important tool for hybrid solar cells a maximum theoretical efficiency of around 33% was obtained by Si-NWs/PEDOT:PSS hybrid solar as demonstrated by Wang et al. in 2016, whereas Yu et al. obtained a practical efficiency of around 13% in the laboratory for Si-NWs/PEDOT:PSS hybrid solar cell containing TAPC.Till date most of the reported works shows that the hybrid solar cells are mainly fabricated by using PEDOT:PSS as the conducting polymer to obtain good efficiency, therefore many challenges are left behind to obtain better results by using variety of conducting polymers. The Si-NWs hybrid solar cell also has the ability to overcome the Schokely-Quisser limit, Hence extreme effort has to be done by the researchers to yield better efficiency of the solar cell device by either changing the polymeric material or the parameters such as the length, height and thickness of Si-NWs.

Acknowledgements The financial support from TMA Pai and Savitri Pai endowment fund is acknowledged. One of the authors Ms. Rabina Bhujel acknowledges for the financial support from above mentioned project.

References

[1] Srinivas B Balaji S Babu M N and Reddy Y S 2015 J. Eng. Res. **3** 178
[2] Saga T 2010 NPG Asia Mater. **2** 96
[3] Carlson D E and Wronski C R 1976 Appl. Phys. Lett. **28** 671
[4] Wu X 2004 Sol. Energy. **77** 803
[5] Kaelin M Rudmann D and Tiwari A N 2004 Sol. Energy. **77** 749
[6] Gur I Fromer N A Geier M L Alivisatos A P 2005 Sci. **310** 462
[7] Ma W Yang C Gong X Lee K and Heeger A J 2005 Adv. Funct. Mater.
[8] Gratzel M 2003 J. Photochem. Photobiol. C. **4** 145
[9] Liu M Johnston M B and Snaith H J 2013 Nature. **501** 395
[10] Yamaguchi M 2003 Sol. Energy Mater. Sol. Cell **75** 261
[11] Liu Z Wang H Fung M K Lee C S and Zhang X H 2013 Chem. Eur. J. **19** 17273
[12] Wagner R S and Ellis W C 1964 Appl. Phys. Lett. **4** 89
[13] Ge J P Wang J Zhang H X and Li Y D 2004 Chem. Eur. **10**, 3525
[14] Swain B S Swain B P and Hwang M N 2010 J. Appl. Phys. **108** 073709
[15] Wu Y Cui Y Huynh L Barrelet C J Bell D C and Lieber C M 2004 Nano Lett. **4** 433
[16] Chehata N Ltaief A Ilahi B Salam B Bouazizi A Maaref H and Beyoud E 2014 Synth. Met.**191** 6
[17] Hochbaum I Fan R He R R and Yang P D 2005 Nano Lett. **5** 457
[18] Eisenhawer B Sensfuss S Sivakov V Pietsch M Andra Gand Falk F 2011 Nanotech.**22** 315401
[19] Yu L O'Donnell B Foldyna M and Cabarrocas P R 2012 Nanotech. **23** 194011
[20] Yu L Fortuna F O'Donnell B Jeon T Foldyna M Picardi G and Cabarrocas P R 2012 Nano Lett. **12** 4153
[21] Hutagalung S D Yaacob K A and Aziz A F A 2007 Appl. Surf. Sci. **254** 633

[22] Davenas J Dkhil S B Cornu D and Rybak A 2012 Energy Proced. **31** 136
[23] Wang H P Lai K Y Lin Y R Lin C A and He J H 2010 Langmuir **26** 1 12855
[24] Peng K Zhang M Lu A Wong N B Zhang R and Lee S T 2007 Appl. Phys. Lett. **90** 163123
[26] Bai F Li M Huang R Li Y Trevora M and Musselman K P 2014 RSC Adv. **4** 1794
[27] Gong X Jiang Y Li M Liu H and Ma H 2015 RSC Adv. **10** 1039
[28] Kurokawa Y Yano M Miyajima S and Yamada A 2017 Jap. J. Appl. Phys. **56** 04CS0
[29] Jiang Y Shen H Zheng C Pu T Wu J Rui C Yang W Y and Li Y 2017 Phys. Status Solidi A **1**
[30] Jung J Y Guo Z Jee S W Um H D Park K T and Lee J H 2010 IEEE
[31] Jeon M and Kamisako K 2009 Mater. Lett. **63** 777
[32] Karaagac H 2014 Phys. Status Solidi A**211** 2503
[33] Kim J Jung C L Kim M Kim S Kang Y Lee H Park J Jun Y and Kim D 2016 The Royal Soc. Chem.
[34] Jiang Y Gong X Qin R Liu H Xia C and Ma H 2016 Nano. Res. Lett. **11** 267
[35] Kalita G Adhikari S Aryal H R Afre R Soga T Sharon M Koichi W and Umeno M 2009 J. Phys. D: Appl. Phys. **42**115104
[36] Ashour E S M Sulaiman M Y Amin N and Ibrahim Z J. Phys. 2013 **436** 012021
[37] Peng K Q Wang X Wu X L and Lee S T 2009 Nano Lett.**9** 3704
[38] Syu H J Shiu S C Lin C F 2011 IEEE 00249
[39] Pham V T Dutta M Bui H T and Fukata N 2014 Adv. Nat. Sci. **5** 045014
[40] Miaoa F Taoa B and Chu P K 2013 Electrochim. Acta **96** 61
[41] Jeon T Geffory B Tondelier D Yu L Jegou P Jousselme B Palacin S Carbarrocas P R I and Bonnassieux Y 2012 Sol. Energy Mater. Sol. Cell.
[42] Woo S Jeong J H Lyu H K Jeong S Sim J H Kim W H Han Y S and Kim Y K 2012 Physica B **407** 3059
[43] Ashour E S M Sulaiman M Y Amin N and Ibrahim Z 2013 J. Phys. **436** 012021
[44] Yu X Shen X Mu X Zhang J Sun B Zeng L Yang L Wu Y He H and Yang D 2015 Scient.Rep. **5** 17371
[45] Lin L Guo S Sun X Feng J and Wang Y 2010 Nanoscale Res. Lett. **5** 1822
[46] Amria C Ouertanib R Hamdia A and Ezzaouiaa H 2017 Mater. Sci. Semicond. Process.176
[47] Sato K Duttaa M and Fukata N 2014 Nanosc. **6** 6092
[48] Sharma M Pudasaini P R Zepeda F R Elam D and Ayon A A 2014 ACS Appl. Mater. Interfaces **6** 4356
[49] Wang W L Zou X S Zhang B Dong J Niu Q L Yin Y A and Zhang Y 2014 Opt. Lett. **39** 3219
[50] Syu H J Subramani T Liu C T Shiu S C and Lin C F 2014 IEEE 1560
[51] Uma K Subramani T Syu H J Lin T C and Lin C F 2015 J. Appl. Phys. **117**, 105102
[52] Wang J X Wang H Prakosoa A B Togonala S A Honga L Jiang C and Rusli 2015 Nanosc. **10** 1039
[53] Gong X Jiang Y Li M Liu H and Ma H 2015 RSC Adv. **10** 1039
[54] Shen X Xia Z Chen L Li S and Zhao J 2016 Electrochem. Acta
[55] Wang H Wang J Hong L Tan Y H Tan C S and Rusli 2016 Nanosc. Res. Lett. **11**311
[56] Yu P Tsai C Y Chang J K Lai C C Chen P H. Lai Y C Tsai P T Li M C Pan H T Huang Y Y Wu C I Chueh Y L Chen S W Du C H Horng S F and Meng H F 2013 ACS Nano **7** 12 10780
[57] Wei W R Tsai M L Ho S T Tai S H Ho C R Tsai S H Liu C W Chung R J and He J H 2013 Nano Lett.**13** 3658
[58] Syu H J Shiu S C and Lin C F 2012 Sol. Energy Mater. Sol. Cell **98** 267
[59] Dkhil S B Bourguiga R Davenas J and Cornu D 2012 Mater. Sci. Eng. B**177** 173
[60] He L Jiang C Rusli Lai D and Wang H 2011 Appl. Phys. Lett. **99** 021104
[61] Shen X Sun B Liu D and Lee S T 2011 J. Am. Chem. Soc. **133** 19408
[62] Eisenhawer B Sensfuss S Sivakov V Pietsch M Andr G and Falk F 2011 Nanotech.**22** 315401
[63] Chehataa N Ltaiefa A Ilahib B Salamc B Bouazizia A Maarefb H and Beyouda E 2014 Synth. Metals.**191** 6

[64] Huang J S Hsiao C Y Syu S J Chao J J and Lin C F 2009 Sol. Energy Mater. Sol. Cell. **93** 621
[65] Yameen M Srivastava S K Singh P Turan K Prathap Vandana P Rauthan C M S and Singh P K 2015 J. Mater. Sci. **50** 8046
[66] Hong L Wang X Zheng H He L Yu H W H and Rusli 2014 Appl. Phys. Lett.**104** 053104